Available online at www.sciencedirect.com
ScienceDirect
Applied Catalysis B: Environmental 78 (2008) 275–287
APPLIED CATALYSIS B: ENVIRONMENTAL
www.elsevier.com/locate/apcatb

Lean reduction of NO by C_3H_6 over Ag/alumina derived from Al_2O_3, AlOOH and $Al(OH)_3$

Runduo Zhang *, Serge Kaliaguine

Department of Chemical Engineering, Laval University, Ste Foy (QC), Canada G1K 7P4

Received 21 December 2006; received in revised form 27 August 2007; accepted 11 September 2007
Available online 20 September 2007

Abstract

The effectiveness of Ag/Al_2O_3 catalyst depends greatly on the alumina source used for preparation. A series of alumina-supported catalysts derived from AlOOH, Al_2O_3, and $Al(OH)_3$ was studied by means of X-ray diffraction (XRD), scanning electron microscopy (SEM), ultraviolet–visible (UV–vis) spectroscopy, diffuse reflectance infrared Fourier transform (DRIFT) spectroscopy, O_2, NO + O_2-temperature programmed desorption (TPD), H_2-temperature programmed reduction (TPR), thermal gravimetric analysis (TGA) and activity test, with a focus on the correlation between their redox properties and catalytic behavior towards C_3H_6-selective catalytic reduction (SCR) of NO reaction. The best SCR activity along with a moderated C_3H_6 conversion was achieved over Ag/Al_2O_3 (I) employing AlOOH source. The high density of Ag–O–Al species in Ag/Al_2O_3 (I) is deemed to be crucial for NO selective reduction into N_2. By contrast, a high C_3H_6 conversion simultaneously with a moderate N_2 yield was observed over Ag/Al_2O_3 (II) prepared from a γ-Al_2O_3 source. The larger particles of Ag_mO ($m > 2$) crystallites were believed to facilitate the propene oxidation therefore leading to a scarcity of reductant for SCR of NO. An amorphous Ag/Al_2O_3 (III) was obtained via employing a $Al(OH)_3$ source and 500 °C calcination exhibiting a poor SCR performance similar to that for Ag-free Al_2O_3 (I). A subsequent calcination of Ag/Al_2O_3 (III) at 800 °C led to the generation of Ag/Al_2O_3 (IV) catalyst yielding a significant enhancement in both N_2 yield and C_3H_6 conversion, which was attributed to the appearance of γ-phase structure and an increase in surface area. Further thermo treatment at 950 °C for the preparation of Ag/Al_2O_3 (V) accelerated the sintering of Ag clusters resulting in a severe unselective combustion, which competes with SCR of NO reaction. In view of the transient studies, the redox properties of the prepared catalysts were investigated showing an oxidation capability of Ag/Al_2O_3 (II and V) > Ag/Al_2O_3 (IV) > Ag/Al_2O_3 (I) > Ag/Al_2O_3 (III) and Al_2O_3 (I). The formation of nitrate species is an important step for the deNO_x process, which can be promoted by increasing O_2 feed concentration as evidenced by NO + O_2-TPD study for Ag/Al_2O_3 (I), achieving a better catalytic performance.

Keywords: SCR; NO; Propene; Silver; Alumina; Boehmite; $Al(OH)_3$; UV–vis; DRIFT; TPD; TPR

1. Introduction

Facing up with the potential energy crisis, the use of lean-burn gasoline engine and diesel engine becomes a popular tendency in order to improve the fuel economy via a more complete combustion of fuel at excess oxygen [1]. NO_x abatement under such oxidizing atmosphere is a great challenge because it requires using the limited reductant to selectively react with NO rather than O_2.

Cu-ZSM-5 was the first catalyst showing promising activity for lean NO_x reduction [2], but the zeolite-based catalysts suffer from low hydrothermal stability and easy deactivation by carbonaceous deposits and SO_2 poisoning [3,4]. Supported-precious metal (such as Pt and Pd) catalysts have an excellent low-temperature activity along with a good resistance to steam and SO_2 poisoning compared to ion-exchanged zeolites [5,6]. Nevertheless, the formation of nitrous oxide, an undesirable greenhouse gas causing global warming, and a narrow temperature range for NO reduction limit their practical application [7,8]. Silver catalysts were deemed as the most effective materials for SCR of NO in excess oxygen and were investigated intensively since 1990s [9–13]. Serving as a support for silver, γ-Al_2O_3 is superior to TiO_2, SiO_2, ZrO_2, TiO_2–ZrO_2 and Ga_2O_3 [14–16]. Moreover, most of reports have already suggested that highly isolated Ag cations, strongly bonded to alumina, are the active sites for NO-SCR process

* Corresponding author. Tel.: +1 418 656 2131 4356.
E-mail address: zhangrd@yahoo.com (R. Zhang).

0926-3373/$ – see front matter.
doi:10.1016/j.apcatb.2007.09.018

[17], whereas metallic silver clusters dominate in the high-silver content alumina-based catalysts, which are less selective for NO reduction and good for the direct combustion of hydrocarbons [18]. Various methods including choosing alumina with smaller pore size and narrower pore-size distribution [19], limiting the silver loading [20], mixing the transition metal precursor with the support precursor in a sol–gel state [21], and leaching out the larger Ag clusters by dilute acid [11], were therefore attempted to prepare a catalyst containing highly dispersed silver. Much attention was paid by previous researchers to correlate the nature of Ag species with their catalytic behaviors as mentioned in literature [11,17,20]. Few reports were however concerned by the relationship between SCR performance and the redox properties of the catalyst.

For the purpose to obtain the best SCR performing catalysts, a colloidal solution containing AlOOH or $Al(OH)_3$ has been employed as a precursor of alumina support in this study. It is hoped that their –OH groups might contribute to Ag species being evenly dispersed and anchored on the alumina surface. Some attractive interaction is also expected during the activation procedure converting Boehmite or aluminum hydroxide to γ-alumina. Ag/Al_2O_3 catalyst was also prepared using commercial γ-Al_2O_3 as a support for a comparative study. The physicochemical properties of prepared catalysts were characterized by X-ray diffraction (XRD), scanning electron microscopy (SEM), ultraviolet–visible (UV–vis) spectroscopy, diffuse reflectance infrared Fourier transform (DRIFT) spectroscopy, O_2 and NO + O_2-temperature programmed desorption (TPD), H_2-temperature programmed reduction (TPR), thermal gravimetric analysis (TGA) and activity test towards NO reduction by propene in the presence of oxygen. Emphasis will be placed on clarifying the relation between the redox properties of the silver catalysts with their catalytic activities for both NO reduction and C_3H_6 oxidation.

2. Experimental

2.1. Preparation method

Alumina-supported silver catalysts were prepared by impregnating the commercial AlOOH (Catapal 18N80), Al_2O_3 (Catabx SBa 150) and $Al(OH)_3$ (Pfaltz & Bauer) supports with an aqueous solution containing desired amounts of silver nitrate (99%, Aldrich) under an intense stirring at room temperature for 4 h. These mixtures were condensed under vacuum using a rotor evaporator (R110, Brinkmann), thereafter, dried at 110 °C for 4 h and calcined at 500 °C for 5 h under a 10% O_2/He gas flow to obtain the final products designated as Ag/Al_2O_3 (I), Ag/Al_2O_3 (II) and Ag/Al_2O_3 (III), respectively. Further calcination of Ag/Al_2O_3 (III) at 800 and 950 °C for 5 h results in the samples denoted as Ag/Al_2O_3 (IV) and Ag/Al_2O_3 (V). Corresponding aluminas (Al_2O_3 (I), Al_2O_3 (II) and Al_2O_3 (III)) were also prepared by the same procedure except for the addition of silver nitrate.

2.2. Physicochemical properties

BET surface areas of the materials were measured by nitrogen adsorption at −196 °C using an automated gas sorption system (NOVA 2000, Quantachrome) operating in continuous mode. The specific surface area was determined from the linear part of the BET curve (P/P_0 = 0.01–0.10). Pore volume and average diameter were obtained from the pore size distribution curve, which was calculated from the desorption branch of N_2 adsorption/desorption isotherms using the Barrett–Joyner–Halenda (BJH) formula.

The Ag contents of the prepared samples were analyzed by atomic absorption spectroscopy (AAS) using a Perkin-Elmer 1100B spectrometer after the samples were dissolved in a mixture of 25 ml of 10% HCl and 2 ml of concentrated HF at 60 °C for 24 h.

Powder X-ray diffraction (XRD) patterns were recorded using a Siemens D 5000 diffractometer and Cu Kα radiation (λ = 1.5406 Å) with a 0.05° step scan from 20 to 80° in 2θ angle. Crystal domain sizes (D) were evaluated by means of the Scherrer equation after Warren's correction for instrumental broadening. The identification of the crystal phases took place using the JCPDS data bank.

The morphologies of alumina-based samples were recorded at 50,000× magnification by scanning electron microscopy (SEM), using a JEOL JSM 840A at 110 kV.

Ultraviolet–visible diffuse reflectance spectra (UV–vis DRS) were collected using a spectrophotometer (Lambda 40, Perkin-Elmer) equipped with a diffuse reflectance attachment (DRA) (Harrick). The UV–vis spectra were collected at room temperature in air in the range of 215–600 nm with a resolution of 2 nm. MgO powder (99.99%, Aldrich) was used as a reference.

Diffuse reflectance infrared Fourier transform (DRIFT) spectra were obtained using a Bio-Rad FTS 60 system fitted with a MCT detector with a resolution of 2 cm^{-1} over the spectral domain of 600–4000 cm^{-1}. A fraction of 10 mg catalyst was diluted into 190 mg KCl (99.99%, Anachemia) and then loaded in the sample holder of a Harrick diffuse reflectance cell.

2.3. Transient analyses

Transient studies were carried out with a multifunctional catalyst testing and characterization system (RXM-100, ASDI), equipped with a quadrupole mass spectrometer (MS) (UTI 100), a thermal gravimetric analyzer (TGA) (CAHN) and a thermal conductivity detector (TCD).

Prior to the TPD of O_2, and NO + O_2, 50 mg samples were treated under an atmosphere of 10% O_2, and 3000 ppm NO + 1% or 10% O_2, respectively, with a total flow rate of 20 cm^3/min at 500 °C for 1 h and then cooled down to room temperature under the same flow, subsequently, flushed with 20 cm^3/min He for 40 min to remove the physisorbed molecules. The temperature was then raised up to 800 °C for O_2-TPD and 500 °C for NO + O_2-TPD at a rate of 10 °C/min. O_2 and NO desorbed during TPD experiments were simultaneously detected and on-line recorded using MS with the mass numbers of 32 and 30, respectively.

Weight changes associated with passing He over Ag/Al_2O_3 (III) were measured as function of time using a TGA. The desorbed H_2O (*m/e* = 18), O_2 (*m/e* = 32), and CO_2 (*m/e* = 44) in the effluent gas were also analyzed by MS.

Prior to H_2-TPR, the samples (50 mg) were pretreated under 10% O_2/He flow at 20 cm^3/min total flow rate (STP) for 1 h at 500 °C, cooled down to room temperature under the same atmosphere, purged with 20 cm^3/min of helium for 40 min to remove the physisorbed O_2, and then heated under a 20 cm^3/min total flow rate of 5% H_2/Ar stream with temperature rising up to 900 °C at a constant heating rate of 5 °C/min. The water in the effluent gas of the TPR process was condensed via a cold trap with a mixture of dry-ice and ethanol. H_2 consumption was monitored continuously by TCD using a flow of 20 cm^3/min of 5% H_2/Ar as reference gas.

The gas responses obtained by MS and TCD during transient studies were calibrated using standard mixtures.

2.4. Activity measurements

The catalytic tests were performed in a fixed-bed reactor under an atmosphere of 1000 ppm NO, 3000 ppm C_3H_6, and 0–10% O_2, balanced by He at a space velocity of 30,000 h^{-1}. The reactor temperature was regulated using a temperature controller (CN3240, Omega) from 200 to 700 °C by steps of 50 °C. The effluent gases (N_2O, NO_2, CO and C_3H_6) were analyzed using a FT-IR gas analyzer (FTLA 2000, ABB). N_2 and O_2 were monitored using a gas chromatograph (GC) (5890, HP) equipped with TCD and separated by columns of molecular sieve 13X and Silicone OV-101. Nitrogen oxides (NO, NO_2) were simultaneously analyzed using a chemiluminescence $NO/NO_2/NO_x$ analyzer (Model 200AH, API). Organo-nitrogen compounds (ONCs), mentioned in the literature as intermediates of NO reduction by hydrocarbons [22–24], can be detected by comparing the different NO_2 values from the NO_x analyzer with that from the IR spectrometer. The higher NO_2 value from the NO_x analyzer was ascribed to the ONCs observed as a NO_2 signal after the NO_2/NO converter of this analyzer. These ONCs were further identified by GC-MS (CP 3800-Saturn 2200, Varian) and confirmed to be mainly composed of $C_3H_7NO_2$ with typical composition of 85–95% $C_3H_7NO_2$, 2–10% $CH_3CH_2NO_2$, ~5% C_2H_5NCO, <2% CH_3ONO and HCN. N_2O yield was not shown in this text due to its limited amount under tested conditions. Nitrogen balance for detected N-containing products (N_2, N_2O, NO_2, and ONCs) was achieved with an error within 5%. Moreover, the global estimate of ONCs content in the effluent gas obtained by GC (from GC/MS) was systematically compared with the values obtained from the difference of NO_x quantification by FTIR and by chemiluminescence. The agreement was found to be within 5% of the estimated value.

3. Results

3.1. Physicochemical properties

The crystal phase analysis was performed by XRD, revealing a main γ-Al_2O_3 phase (JCPDS 29-0063) for Al_2O_3(I) and Al_2O_3 (II), suggesting that γ-alumina structure can be formed whether using Boehmite or γ-Al_2O_3 as Al source for support via the present preparation method after a 500 °C calcination. The XRD patterns of silver-loaded samples Ag/Al_2O_3 (I) and Ag/Al_2O_3 (II) did not contain any visible additional peaks corresponding to Ag_2O (JCPDS 41-1104) or Ag^0 (JCPDS 04-0783) with respect to their parent aluminas. An explanation for this phenomenon is that the loaded silver was very well dispersed over the alumina substrate. Al_2O_3 (III) and Ag/Al_2O_3 (III) were synthesized from the $Al(OH)_3$ source and were calcined at 500 °C, exhibiting an amorphous structure in their XRD profiles. A γ-phase alumina was obtained via further thermal treatment of Ag/Al_2O_3 (III) at 800 and 950 °C, respectively, as shown in the XRD patterns for Ag/Al_2O_3 (IV) and Ag/Al_2O_3 (V). High-temperature calcination is indeed necessary for ensuring a good crystallization of the γ-phase Al_2O_3 when $Al(OH)_3$ is used as Al source.

According to previous reports the formation of $AgAlO_2$ (JCPDS 21-1070) is realized by hydrothermal treating 1–5 wt% Ag/Al_2O_3 at 800 °C [25] or calcining 21.5 wt% Ag/Al_2O_3 at 850 °C [11]. In addition, Bogdanchikova et al. pointed out the generation of a $AgAl_{11}O_{17}$ phase (JCPDS 80-0997) in 10 wt% Ag/Al_2O_3 [26]. The two samples of Ag/Al_2O_3 (IV) and Ag/Al_2O_3 (V) were submitted to a high-temperature calcination in this study. Unfortunately, the ascription of those XRD lines belonging to silver aluminates in the 2θ range of 33–36° has not been ascertained because the carrier alumina exhibits some diffraction peaks at these positions, making it difficult to discern peaks due to silver aluminates. Further proof besides the data from XRD to clarify the existence of silver aluminates is deemed to be necessary.

SEM pictures show that Al_2O_3 (I) clusters are almost regular spheres with diameters of 30–200 nm. The morphology hardly changes after Ag impregnation of Al_2O_3 (I). Irregular clusters with a severe agglomeration were observed in the SEM pattern of amorphous Ag/Al_2O_3 (III) in accordance with its low pore volume (as evidenced by N_2 adsorption), while a better alumina dispersion was found in the case of Ag/Al_2O_3 (IV).

BET specific surface area, pore volume & size, crystallite size and Ag content of prepared alumina-based catalysts are summarized in Table 1. The Ag loadings of silver-containing samples determined by AAS are close to a value of 3 wt%. Ag/Al_2O_3 (I) with various loadings of 1–6 wt% besides 3 wt% was also synthesized in order to investigate the effect of Ag loading on catalytic performance (not shown in Table 1). The supports originating from AlOOH or γ-Al_2O_3 and denoted as Al_2O_3 (I) or Al_2O_3 (II) display a high surface area of ~140 m^2/g. Ag loading over these two carriers scarcely affects the values of their surface areas. By contrast, a relatively lower surface area (about 64 m^2/g) was found for Al_2O_3 (III) prepared from $Al(OH)_3$. Subsequently, Ag impregnation further decreased its surface area achieving a value of 35 m^2/g. The surface area of Ag/Al_2O_3 (III) was significantly enhanced by means of calcinations at 800 and 950 °C reaching values of 79 m^2/g for Ag/Al_2O_3 (IV) and 61 m^2/g for Ag/Al_2O_3 (V). Taking into account the XRD data which show a transformation from the amorphous phase for Ag/Al_2O_3 (III) to γ-Al_2O_3 phase for Ag/

Table 1
Physicochemical properties of alumina-based catalysts

Sample	Specific surface area (m^2/g)	Pore volume (ml/g)	Pore size (nm)	Crystal domain size (nm)	Ag weight percent (%)
Al_2O_3 (I)	143	0.42	11.9	7.7	–
Ag/Al_2O_3 (I)	140	0.40	10.8	6.6	2.9
Al_2O_3 (II)	144	0.47	9.5	6.8	–
Ag/Al_2O_3 (II)	144	0.47	9.5	6.9	3.1
Al_2O_3 (III)	64	0.26	3.8	–	–
Ag/Al_2O_3 (III)	35	0.15	3.8	–	3.2
Ag/Al_2O_3 (IV)	79	0.22	10.8	7.9	3.1
Ag/Al_2O_3 (V)	61	0.22	14.6	6.8	3.1

Al_2O_3 (IV) and Ag/Al_2O_3 (V), the formation of the gamma alumina phase is deemed as the main reason for the enhancement in surface area. The higher pore volumes of Al_2O_3 (I and II) with or without Ag loading (0.4–0.5 ml/g) coincide with their higher surface areas compared to the other samples. Furthermore, those samples representing a γ-Al_2O_3 structure (Ag/Al_2O_3 (I, II, IV, V) and Al_2O_3 (I, II)) have larger pore sizes of 9–15 nm. The opposite occurs on amorphous samples (Ag/Al_2O_3 (III) and Al_2O_3 (III)) with pore sizes of ~3.8 nm. Based on SEM results, the agglomeration of Ag/Al_2O_3 (III) is thought to contribute to the small pore size of those catalysts. With the further condensation of –OH groups simultaneously with the formation of γ-Al_2O_3 phase at higher temperatures (800 or 950 °C), the pore size was markedly improved accompanying the increase of surface area and the formation of γ-Al_2O_3 phase. Among the catalysts with γ-Al_2O_3 structure, the surface areas of Ag/Al_2O_3 (IV, V) are lower than those of Ag/Al_2O_3 (I, II) likely related to the lower pore volumes (about 0.2 ml/g) of the formers. As seen from Table 1, the crystal domain sizes of alumina were also calculated as ~7 nm based on XRD peak at $2\theta \approx 66.8^\circ$.

The existence of different oxidation states of silver was demonstrated through UV–vis DRS (Fig. 1). In the spectra of Ag/Al_2O_3 (I, II and III), a sole band appears at 220–240 nm. A similar band has been observed for Ag/Al_2O_3 [11,12] and Ag^+/H-ZSM-5 [27], and was assigned to the Ag^+ ions or Ag_2O nanoparticles highly dispersed on the support. Moreover, the contribution from the alumina substrate displaying weak UV–vis bands around 220 nm (not shown) should also be considered. There are shoulders at 340 nm for Ag/Al_2O_3 (II), 300 and 355 nm for Ag/Al_2O_3 (IV), believed to correspond to the oxidized silver clusters (Ag_n^+) [12,28–30]. In addition to Ag^+ (220 nm) and Ag_n^+ (290 and 355 nm) peaks, a peak at 425 nm, attributed to Ag^0 in the literature [12,28], was also visible in the spectrum of Ag/Al_2O_3 (V).

DRIFT spectra of Al_2O_3 (I, II) and Ag/Al_2O_3 (I–V) are shown in Fig. 2. The intense peaks at 1550, 1483, 1377 cm^{-1} located in the carbonate region [31], associated with a peak of 2348 cm^{-1} well known as corresponding to adsorbed CO_2 were observed in the DRIFT plot of Ag/Al_2O_3 (III). This result reflects the fact that some carbonaceous organic compounds may exist in the $Al(OH)_3$ precursor causing the generation of carbonate species via an oxidation process during the calcination of Ag/Al_2O_3 (III) at 500 °C. It was noticed that these carbonate species could be effectively eliminated via a high-temperature treatment as indeed observed in the DRIFT spectra for Ag/Al_2O_3 (IV and V). A broad band at 3552 cm^{-1} was observed for all investigated samples, which was assigned to isolated surface Al–OH groups [32]. A clear decrease in intensity occurred in the region of hydroxyl groups for Ag/

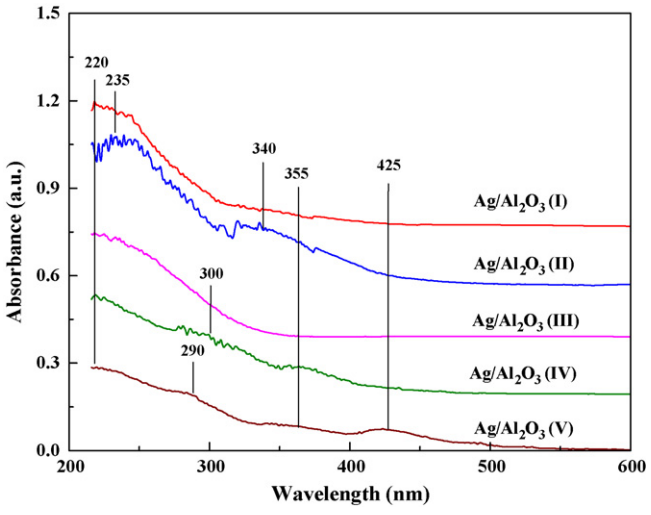

Fig. 1. UV–vis spectra of Ag/Al_2O_3 (I–V) samples.

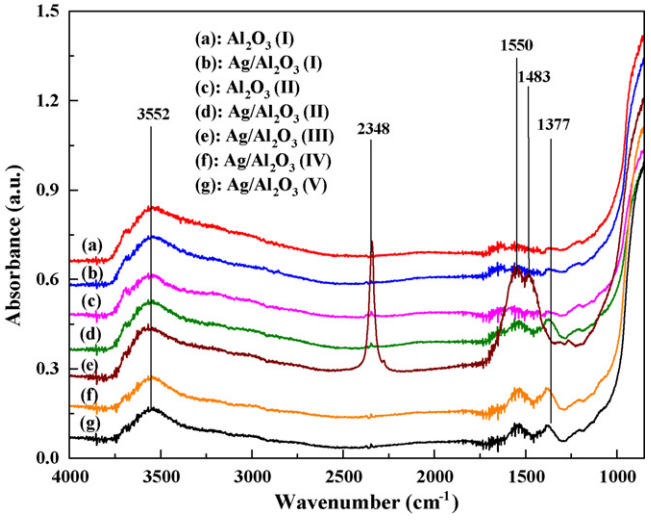

Fig. 2. DRIFT spectra of Al_2O_3 (I, II) and Ag/Al_2O_3 (I–V) samples.

Al_2O_3 (IV and V) compared to that for Ag/Al_2O_3 (III), in accordance with a diminution in the number of –OH groups after calcining at higher temperatures.

3.2. Temperature programmed analysis

The oxygen species formed over alumina-based catalysts after 10% O_2 adsorption were investigated by O_2-TPD experiments, as illustrated in Fig. 3a and b. The amount of O_2 released from solid solutions was calculated after integration of the O_2 desorption curve and reported in Table 2. A single O_2 desorption of 4.2 μmol/g occurs over Al_2O_3 (I) at high-temperature (736 °C). As seen from line (b) for Ag/Al_2O_3 (I) in Fig. 3a, Ag loading significantly enhanced the O_2 adsorption, yielding a major peak (14.2 μmol/g) at 693 °C. O_2-TPD profile for Al_2O_3 (II) was slightly shifted to lower temperature (640 °C) and showed a little higher O_2 desorption (6.3 μmol/g) compared to that for Al_2O_3 (I). It is clear from the comparison of lines (c) and (d) in Fig. 3a that the loading of Ag over γ-phase Al_2O_3 (II) not only promoted the high-temperature O_2 desorption (9.6 μmol/g at 646 °C) but also resulted in a new low-temperature peak (1.4 μmol/g at 404 °C). A large amount of O_2 was desorbed from Al_2O_3 (III) (113 μmol/g) and Ag/Al_2O_3 (III) (194 μmol/g) in the temperature region of 500–800 °C as depicted by line (e) and (f) in Fig. 3b. Nevertheless, this feature is not longer observable after calcination of Ag/Al_2O_3 (III) at 800 °C for 5 h (line (g) in Fig. 3b for Ag/Al_2O_3 (IV)). As a result, the O_2 uptake from Ag/Al_2O_3 (IV) during O_2-TPD is reduced to 9.7 μmol/g. Fig. 3c reports a detailed study of TPD behaviors along with a TGA for Ag/Al_2O_3 (III) showing a drastic loss of catalyst weight simultaneously with the desorption of O_2, CO_2 and H_2O molecules at 600–800 °C. These molecules are believed

Table 2
Amount of O_2 desorbed from the alumina-based samples during O_2-TPD experiments

Sample	Amount of oxygen desorbed	
	Low-temperature (μmol/g)	High-temperature (μmol/g)
Al_2O_3 (I)	–	4.2 (736 °C)
Ag/Al_2O_3 (I)	–	14.2 (693 °C)
Al_2O_3 (II)	–	6.3 (640 °C)
Ag/Al_2O_3 (II)	1.4 (404 °C)	9.6 (646 °C)
Al_2O_3 (III)	–	113.4 (688 °C)
Ag/Al_2O_3 (III)	–	193.8 (717 °C)
Ag/Al_2O_3 (IV)	1.6 (<500 °C)	8.1 (>500 °C)

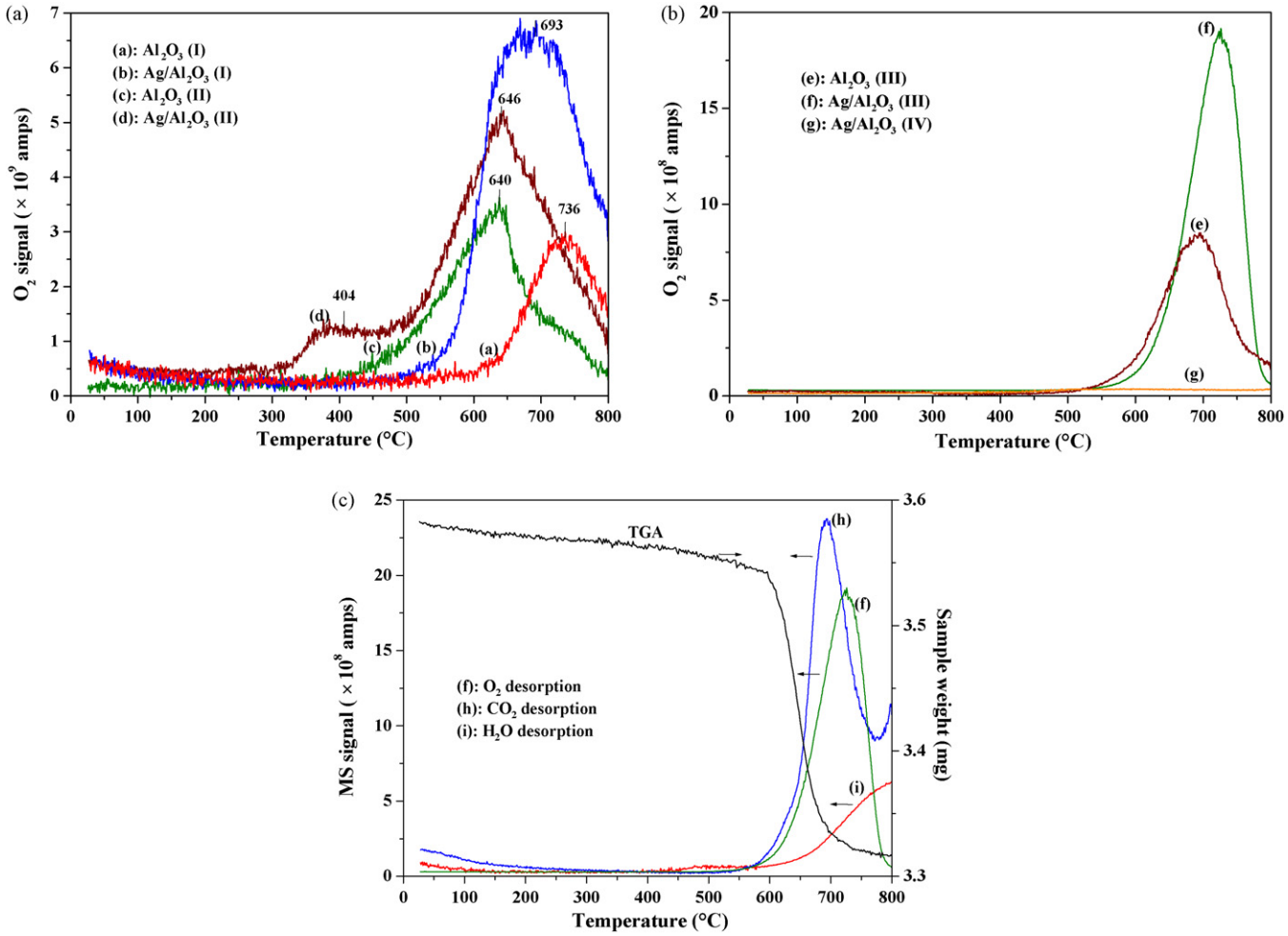

Fig. 3. (a) O_2-TPD profiles of Al_2O_3 (I), Ag/Al_2O_3 (I), Al_2O_3 (II) and Ag/Al_2O_3 (II) samples, (b) O_2-TPD profiles of Al_2O_3 (III), Ag/Al_2O_3 (III) and Ag/Al_2O_3 (IV) samples, (c) TGA profile of Ag/Al_2O_3 (III) sample under He.

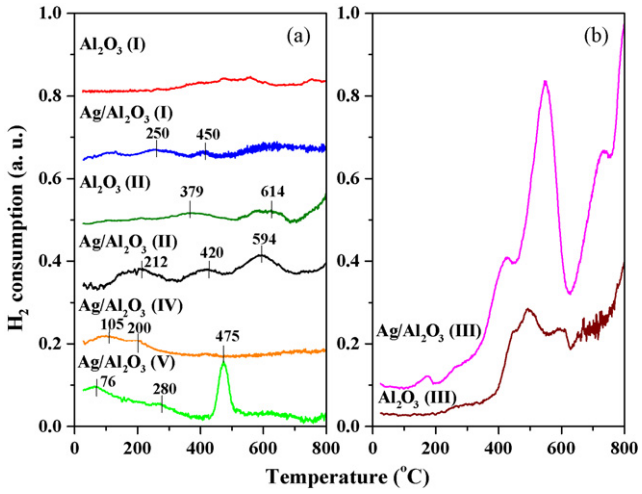

Fig. 4. H_2-TPR profiles of alumina-based samples.

to be released from lattice in light of their high desorption temperature and large desorbed amounts simultaneously with a phase transformation as evidenced by XRD. Moreover, the existence of carbonate species in Ag/Al_2O_3 (III) as verified by its DRIFT spectrum (Fig. 2) is responsible for the large amount of CO_2 desorbed.

The reducibility of the prepared solids was investigated by H_2-TPR experiments. The results are shown in Fig. 4a and b. Al_2O_3 (I) is hardly reducible at $T < 800$ °C implying its good stability even under a reducing atmosphere, while multiple light peaks appear in the region of 100–500 °C in the TPR curve for Ag/Al_2O_3 (I). For Al_2O_3 (II) alone, a minor H_2 consumption peak at 379 °C and two subsequent ones at 614 and >695 °C (likely due to the reduction of some minor surface impurities) was found (Fig. 4a). An additional peak occurs at 212 °C followed by others at 420, 594 and >698 °C in the TPR plot of Ag/Al_2O_3 (II) with respect to the parent Al_2O_3 (II). A TPR peak with a maximum at 105 °C appears in the case of Ag/Al_2O_3 (IV). Interestingly, not only a significant H_2 consumption at low-temperatures (76 and 280 °C) but also a sharp one at 475 °C occurs over Ag/AlO_3 (V) during the H_2-TPR test. With respect to Al_2O_3 (I and II) and Ag/Al_2O_3 (I, II, IV and V) having γ-phase structure, more intense multiple-step reduction at $T > 300$ °C was apparent in Fig. 4b for amorphous Al_2O_3 (III) and Ag/Al_2O_3 (III). The peaks observed for Al_2O_3 (III) are associated with the reaction of the surface carbonates discussed above as reflected by the presence of CO_2 ($m/e = 44$) in the TPR effluent gas.

The NO desorption ($m/e = 30$) during the TPD process after the coadsorption of NO/O_2 over Ag/Al_2O_3 (I) was quantified through a deconvolution of the desorption profiles using Lorentzian peak fitting. The adsorption of 3000 ppm NO and 1% O_2 resulted in one major peak (8.6 μmol/g) at 179 °C and another minor one (2.1 μmol/g) at 354 °C. This feature of NO peak was drastically changed upon increasing the O_2 concentration up to 10% O_2. As a result, the high-temperature NO peak desorbed from Ag/Al_2O_3 (I) was significantly enhanced during TPD experiments exhibiting an intense NO peak (42.3 μmol/g) at 383 °C associated with one peak (3.9 μmol/g) at 67 °C and its shoulder (1.8 μmol/g) at 155 °C.

3.3. Activity tests

3.3.1. Conditions in excess O_2

The temperature dependence of NO conversion to N_2 in a feed flow of 1000 ppm NO + 3000 ppm C_3H_6 + 10% O_2 over Al_2O_3 (I) and Ag/Al_2O_3 (I–V) is depicted in Fig. 5a. For alumina alone, N_2 yield was marginal unless $T > 400$ °C and then increased rapidly at increasing temperature reaching a maximum of 76% at 500 °C, eventually, declined into 23% at 600 °C. With the addition of silver to alumina, the best performance for NO selective reduction to N_2 was obtained over Ag/Al_2O_3 (I) giving a N_2 yield of 74% at a temperature as low as 300 °C and achieving values of more than 90% over a wide temperature range with a plateau from 350 to 550 °C. A moderate N_2 yield over Ag/Al_2O_3 (II) was observed starting at 200 °C and passing through the maximum of 84% at 450 °C, before gradually declining at relatively higher temperature. A plot of N_2 yield similar to that for pure Al_2O_3 (I) was found for Ag/Al_2O_3 (III) displaying obvious SCR activity solely at $T > 400$ °C and showing a maximum N_2 yield of 60% at 500 °C. In the case of Ag/Al_2O_3 (IV) synthesized by calcining Ag/Al_2O_3 (III) at 800 °C, a good N_2 yield at low-temperature (300–400 °C) and its progressive diminution at elevating temperature (400–600 °C) were observed. The worst N_2 yield was obtained over Ag/Al_2O_3 (V) with values around 20% in the range of 300–450 °C and level off at >600 °C.

At low-temperature (200–400 °C) organo-nitrogen compounds (ONCs) due to the partial conversion of NO were detectable in the effluent and showed yields in the following order: Ag/Al_2O_3 (I) > Ag/Al_2O_3 (IV) > Ag/Al_2O_3 (II) > Al_2O_3 (I), Ag/Al_2O_3 (III), Ag/Al_2O_3 (V) as illustrated in Fig. 5b. The obvious ONCs yield over Al_2O_3 (I) and Ag/Al_2O_3 (III) can only be obtained at $T > 500$ °C with maxima of 34% and 28%, respectively. NO_2, another kind of nitrogen-containing by-product, was observed at temperatures above 500 °C showing a trend of Ag/Al_2O_3 (II, IV and V) > Ag/Al_2O_3 (I) > Ag/Al_2O_3 (III) > Al_2O_3 (I), as illustrated in Fig. 5c. The NO conversion curves (Fig. 5d) were similar to N_2 yield curves (Fig. 5a) for silver catalysts, reflecting the high selectivity towards N_2 during SCR reaction.

The temperature dependence of C_3H_6 conversion on temperature during NO-SCR is shown in Fig. 5e. The relatively lower C_3H_6 conversions were achieved over Al_2O_3 (I) and Ag/Al_2O_3 (III) with a light-off at ca. 400 °C. These conversions keep going on with temperature and up to almost 100% at 600 °C. On the contrary, the best conversion of C_3H_6 occurred over Ag/Al_2O_3 (II) showing a 90% C_3H_6 conversion even at relatively lower temperature of 300 °C followed by a complete conversion at temperature higher than 450 °C. A C_3H_6 conversion comparable to that for Ag/Al_2O_3 (II) was also obtained in the case of Ag/Al_2O_3 (V). In addition, the moderate C_3H_6 conversion among the tested six samples was found over Ag/Al_2O_3 (IV) and Ag/Al_2O_3 (I) with values of 70% and 57% at 400 °C, respectively. Some CO formation took place over Ag/Al_2O_3 (I) in the temperature region of 250–600 °C with a maximum of 12% at 450 °C, while a significant CO yield was

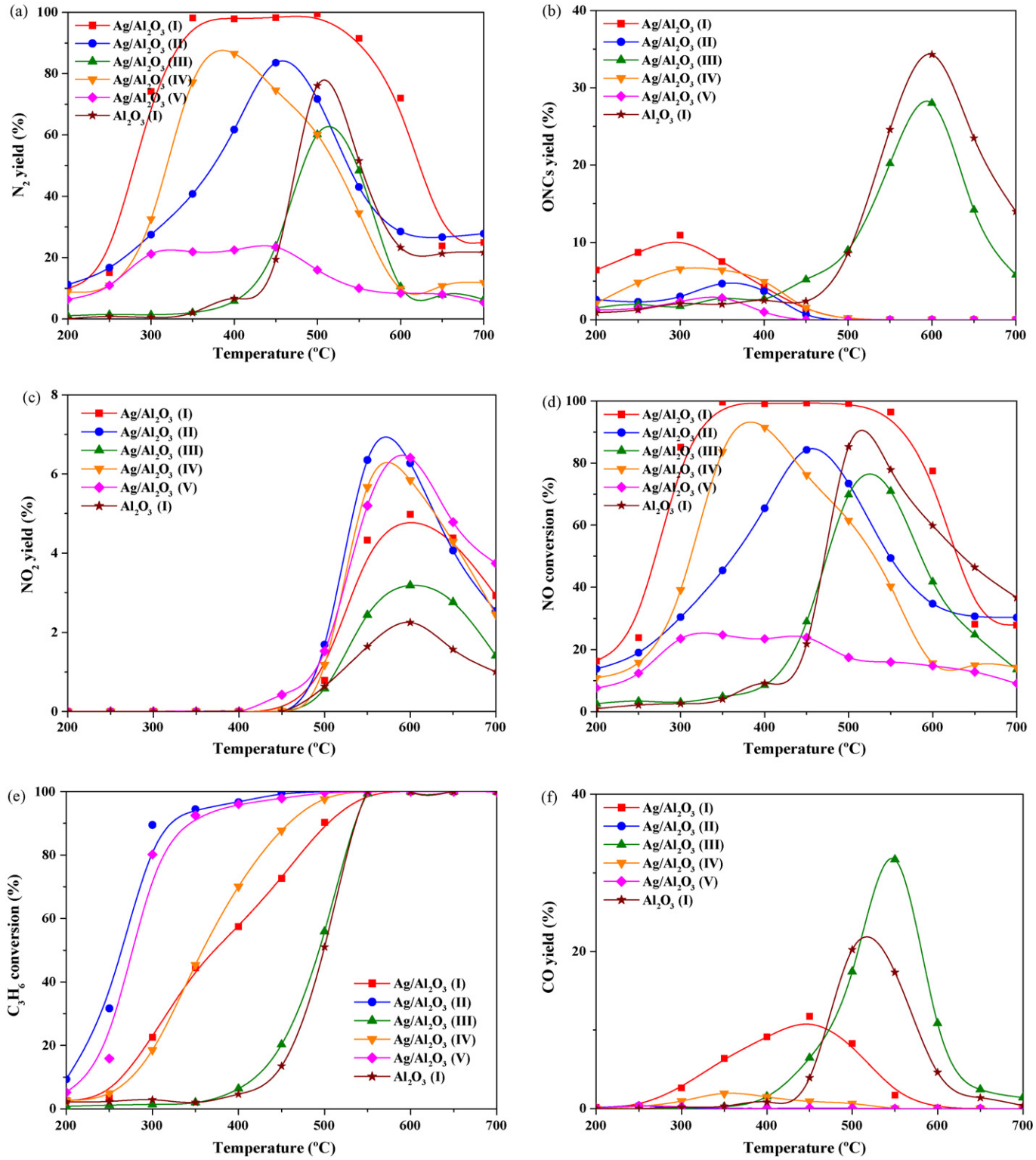

Fig. 5. (a) N_2 yield; (b) ONCs yield; (c) NO_2 yield; (d) NO conversion; (e) C_3H_6 yield; (f) CO yield in C_3H_6-SCR of NO over alumina-based samples. Conditions: GHSV = 30,000 h^{-1}, 1000 ppm NO, 3000 ppm C_3H_6, 10% O_2.

found for Ag/Al_2O_3 (III) and Al_2O_3 (I) at relatively higher temperatures, reaching maxima of 32% at 550 °C and 20% at 500 °C, respectively, as shown in Fig. 5f. The CO yield obtained over Ag/Al_2O_3 (IV) is minor at 250–550 °C, whereas Ag/Al_2O_3 (V) showed no CO formation.

3.3.2. Oxygen close to stoichiometry

The catalytic performance in terms of N_2, ONCs, NO_2 and CO yields, along with NO and C_3H_6 conversions in the SCR of NO by propene in the presence of 1% O_2 over the best performing catalyst Ag/Al_2O_3 (I) was also investigated with the

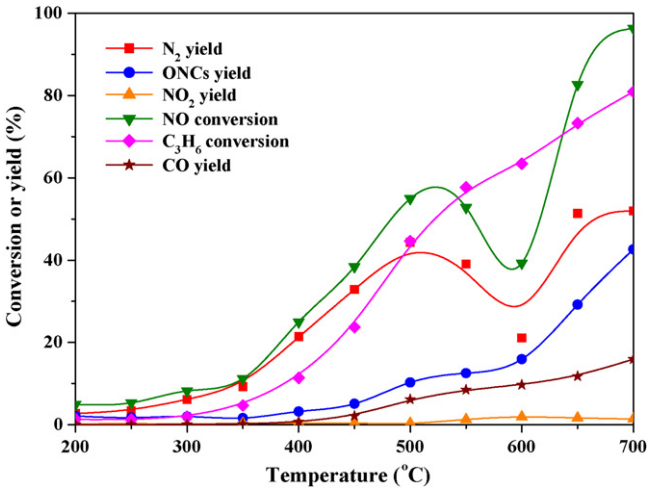

Fig. 6. Catalytic performance of Ag/Al_2O_3 (I) in C_3H_6-SCR of NO. Conditions: GHSV = 30,000 h^{-1}, 1000 ppm NO, 3000 ppm C_3H_6, 1% O_2.

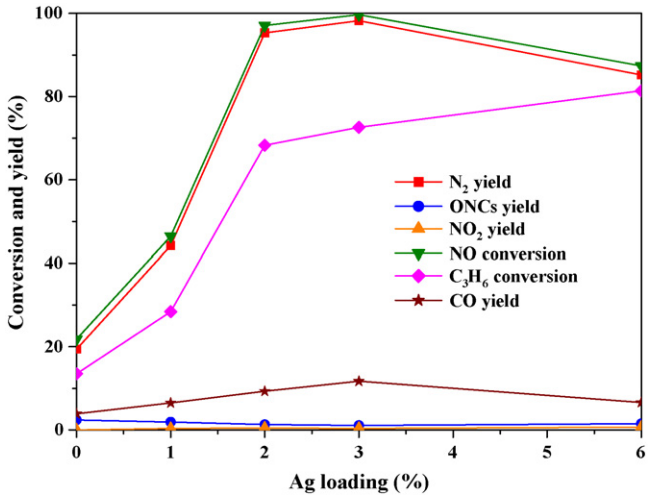

Fig. 8. Effect of Ag loading on catalytic behavior over Al_2O_3 (I) supported samples. Conditions: GHSV = 30,000 h^{-1}, 1000 ppm NO, 3000 ppm C_3H_6, 10% O_2, 450 °C.

results being reported in Fig. 6. A maximum N_2 yield of 44% at 500 °C and another one of 52% at 700 °C were observed. A progressive increase in C_3H_6 conversion is found with the increase of temperature up to 81% at 700 °C. These values for N_2 yield and C_3H_6 conversion in Fig. 6 are quite inferior to those obtained in the presence of 10% O_2 over the same catalyst (compare to Fig. 5a and e). The C_3H_6-SCR of NO in 1% O_2 was also performed over Al_2O_3 (I) showing a N_2 yield comparable to that obtained over Ag/Al_2O_3 (I) at >600 °C although this Al_2O_3 (I) is essentially inactive for NO reduction to N_2 at low-temperature (not shown). The ONCs and CO yields achieved over Ag/Al_2O_3 (I) were also promoted at high-temperature, leading to the respective maxima of 43% and 16% at 700 °C.

3.3.3. Effect of O_2 feed concentration

N_2, ONCs, NO_2 and CO yields; as well as NO and C_3H_6 conversions as functions of O_2 feed concentration over Ag/Al_2O_3 (I) at 500 °C are shown in Fig. 7. N_2 yield was rather poor (14%) in the absence of oxygen, however, it increased dramatically upon O_2 feed concentration and exceeded 97% at >4% O_2. C_3H_6 conversion was also promoted by oxygen. Along with the rapid increase in N_2 yield and C_3H_6 conversion in the O_2 range of 0–4%, the formation of ONCs was observed with a maximum of 10% at 2% O_2 before declining at higher oxygen concentrations. A small oxygen content (2%) seems enough to facilitate the CO production achieving a value of ~8%. NO_2 generation was hardly observed under the test conditions.

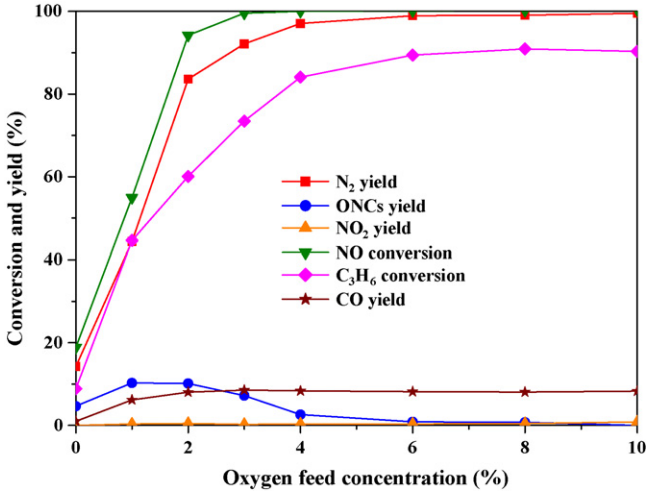

Fig. 7. Effect of O_2 feed concentration on catalytic behavior over Ag/Al_2O_3 (I). Conditions: GHSV = 30,000 h^{-1}, 1000 ppm NO, 3000 ppm C_3H_6, 500 °C.

3.3.4. Effect of Ag loading

NO reduction by C_3H_6 in the presence of 10% O_2 was also performed over alumina-based catalysts with various Ag loadings (0–6 wt%) at 450 °C, as illustrated in Fig. 8. Ag-free sample catalytic activity is low showing a 19% N_2 yield and a 14% C_3H_6 conversion. With the addition of 1 wt% Ag, both N_2 yield and C_3H_6 conversion were obviously improved yielding values of 44% and 28%, respectively. The optimal Ag loading was found to be 2–3 wt% resulting in a N_2 yield of >95% and C_3H_6 conversion of ~70%. CO yield was maximum at 3 wt% Ag loading. Further increase of the Ag content led to a decline in N_2 (85%) and CO yields (7%) whereas C_3H_6 conversion was increased (81%).

4. Discussion

4.1. Redox properties

Bulk Ag_2O is known to decompose thermally into metallic Ag even at a temperature as low as 250 °C [33]. However, nanoscale Ag_2O can be stabilized by high-surface-area alumina through a strong interaction which maintains the silver in a higher oxidation state, as evidenced by the catalyst color, ultraviolet–visible (UV–vis) spectroscopy, and X-ray absorption fine structure (XAFS) [11,12,32]. Authors also pointed out that Ag_2O size increased at high loading for alumina-supported

silver, while large particle size Ag_2O would become unstable and be decomposed into Ag and O_2. High-temperature is beneficial for this Ag_2O decomposition.

The quantification of H_2 consumption taking place during H_2-TPR of Ag/Al_2O_3 (I, II, IV and V) shows values falling into the range of 60–150 μmol/g catalyst, which match well with the H_2 amount for corresponding silver oxides reduction (139 μmol/g catalyst) and is far lower than the value needed for complete depletion of the lattice oxygen of Al_2O_3 (29412 μmol/g catalyst). This indicates that only a fraction of Ag/Al_2O_3 (I, II, IV, and V) was reduced, likely located over the surface. In addition, TPR seems to be an effective method to study the reducibility of lattice oxygen related to various Ag species, which was distinguished by their different peak positions. Richter et al. once prepared series of Ag/Al_2O_3 using the impregnation method and found that the main hydrogen consumption at ∼290 °C for an Ag content of 5 wt% was systematically shifted to higher temperatures with decreasing Ag loading [34]. Taking into account the fact that small silver oxide clusters prevail in the case of low Ag surface concentrations over alumina [11,32], Richter's observation suggests that the Ag_2O clusters are increasingly stabilized against reduction along with the diminution in their particle sizes at decreasing Ag loading. Based on the previous literature assignment and the essential nature of support precursor, the minor H_2 consumption at 250 °C in the TPR pattern for Ag/Al_2O_3 (I) (Fig. 4a) was likely ascribed to the reduction of fine Ag_2O particles, while those occurring at >360 °C were mainly attributed to those Ag^+ cations evenly distributed over the alumina matrix. Both Ag_2O nanopaticles and Ag^+ cations of Ag/Al_2O_3 (I) display as a UV–vis band at around 220 nm in Fig. 1. The low-temperature peak at 212 °C in the TPR profile of Ag/Al_2O_3 (II) was related to silver oxide clusters, likely appearing as an Ag_n^+ band at 340 nm in the UV–vis spectrum, whose sizes become bigger according to the shift of the TPR peak to low-temperature compared to Ag/Al_2O_3 (I). The peak at 420 °C was assigned to Ag^+ ions highly dispersed over the γ-Al_2O_3 support. Finally, the TPR peaks at 594 °C and >703 °C for Ag/Al_2O_3 (II) were associated with the two H_2 consumptions at 614 °C and >695 °C for Al_2O_3 (II). They were accordingly assigned to the depletion of lattice oxygen from the surface alumina substrate or surface carbonate species. A reduction occurring at relatively low-temperature in the case of Ag/Al_2O_3 (IV) (105 °C) and Ag/Al_2O_3 (V) (76 °C) was found during TPR experiments, indicating that the size of silver oxide clusters over the surface became even larger. These clusters become unstable with their increasing size because of the weaker interaction with the alumina substrate. This causes a partial decomposition of Ag_2O due to its low thermal stability: $Ag_2O \rightarrow 2\ Ag + 1/2\ O_2$. Especially, the Ag_2O decomposition into metallic Ag occurring over Ag/Al_2O_3 (V) became apparent enough to be detected by UV–vis (Fig. 1). Hence, the cluster of silver oxides with a relatively large size in the case of Ag/Al_2O_3 (II, IV, and V) would rather be formulated as Ag_mO ($m > 2$) than Ag_2O. The sharp reduction peak at 475 °C in the TPR plot of Ag/Al_2O_3 (V) reflects a sudden destruction of certain crystal structure under a 5% H_2/Ar atmosphere. The formation of a silver aluminate phase by thermal or hydrothermal treating of Ag/Al_2O_3 catalysts was previously documented [11,25,26]. For example, Bogdanchikova et al. thought that about a quarter of the silver was in the form of silver aluminate crystallites in a fresh 10 wt% Ag-containing Al_2O_3 catalyst [26]. Considering the preparation of Ag/Al_2O_3 (V) which involves a calcination temperature as high as 950 °C, the formation of silver aluminate phase in this catalytic material is possible. This H_2 consumption at 475 °C for Ag/Al_2O_3 (V) was therefore attributed to the reduction of silver aluminate crystallites yielding metallic silver.

Various oxygen species on the silver surface were previously investigated by Raman spectroscopy and roughly classified into physisorbed molecular oxygen, chemisorbed molecular oxygen ($Ag–O_2$) and the ionic oxygen incorporated into the substrate [35]. In the present study, only one O_2 peak for Al_2O_3 (I) occurring at 736 °C was likely related to the liberation of surface lattice oxygen associated with aluminum (Al–O) (line (a) in Fig. 3a). A clear enhancement in the intensity of this O_2 peak after Ag loading, as seen from line (b) in Fig. 3a for Ag/Al_2O_3 (I), may be explained by the incorporation of silver into lattice to form an Ag–O–Al structure, which is likely more reducible than an Al–O–Al structure. The O_2 desorption occurring at 640 °C over Al_2O_3 (II) was again assigned to the release of lattice oxygen bound to aluminum (line (c) in Fig. 3a). In the profile of O_2-TPD for Ag/Al_2O_3 (II), the O_2 desorption appearing at 646 °C was accordingly attributed to the lattice oxygen associated with silver or aluminum, whereas, another O_2 desorption at 404 °C was assigned to the molecular oxygen chemisorbed upon silver due to its low desorption temperature falling into the temperature range for α-oxygen desorption as previously described in Ref. [36] (line (d) in Fig. 3a). An attempt was made to correlate the distinct O_2-TPD behaviors of Ag/Al_2O_3 (I) and Ag/Al_2O_3 (II) with the nature of their alumina sources (Ag/Al_2O_3 (I) was prepared from a Boehmite, while Ag/Al_2O_3 (II) was prepared from γ-phase Al_2O_3). During the preparation procedure for Ag/Al_2O_3 (I), an exchange between –OH groups of Boehmite and Ag^+ ions of silver nitrate might take place, which is favorable to the formation of an Ag–O–Al local structure and the high dispersion of Ag over alumina:

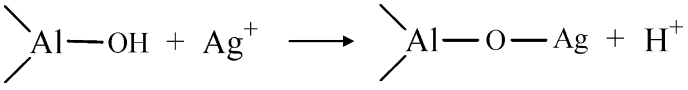

As for the preparation of Ag/Al_2O_3 (II), the chance to yield Ag–O–Al structure is reduced due to the scarcity of hydroxyl group over γ-phase alumina compared to Boehmite. The higher lattice oxygen desorption at 646 °C for Ag/Al_2O_3 (II) (9.6 μmol/g) compared to that at 640 °C for parent Al_2O_3 (II) (6.3 μmol/g) could be ascribed to the contribution from the highly dispersed Ag_2O particles over the surface, having a strong interaction with support, or Ag^+ ions associated with lattice oxygen. The low-temperature peak at 404 °C in the O_2-TPD profile for Ag/Al_2O_3 (II) reflects its peculiar redox characteristic. The formation of some larger Ag_mO ($m > 2$) clusters over Ag/Al_2O_3 (II) is supported by the TPR (Fig. 4a)

and UV–vis results (Fig. 1). The increasing particle size can accelerate the metallic Ag yield due to Ag_2O decomposition. Moreover, the stability of Ag_mO clusters will decrease because of a relatively poor interaction with alumina with the increase of their sizes. The above reasons seem to explain this O_2 desorption appearing at relatively low-temperature. The O_2 desorbed from perovskites at similar temperatures was previously designated as α-O_2, and was thought to be crucial for hydrocarbons oxidation in this case [36–38]. It is also possible that the rates of hydrocarbon oxidation are dependent on Ag particle size with higher rates being associated with larger particles [29,39]. Hence, Ag/Al_2O_3 (II) was expected to achieve a better activity for C_3H_6 oxidation.

A shift of O_2 desorption peak to lower temperature was found for Al_2O_3 (I) after Ag loading, while Ag impregnation over Al_2O_3 (II) does not affect the desorption temperature significantly. This again suggests that the loaded Ag was mostly incorporated into Al_2O_3 (I) whereas it mainly existed as dispersed silver oxides over Al_2O_3 (II) in accordance with our assumption based on UV–vis and TPR results (Figs. 1 and 4a).

It was observed from Fig. 3b and Table 2 that large amounts of O_2 were desorbed from amorphous Al_2O_3 (III) at 688 °C compared to Al_2O_3 (I and II). Additionally, a significant O_2 desorption (194 μmol/g) occurred over Ag/Al_2O_3 (III) along with CO_2 and H_2O desorption at $T > 600$ °C. This was found to be associated with a sudden almost 10% loss in weight as established by TGA (Fig. 3c). Similarly, an intense H_2 consumption also took place in the case of Al_2O_3 (III) and Ag/Al_2O_3 (III) as described by TPR profiles in Fig. 4b. Interestingly, Ag/Al_2O_3 (IV) having a γ-phase Al_2O_3 structure, obtained by means of calcining the amorphous Ag/Al_2O_3 (III) at 800 °C, shows a comparable O_2 desorption (9.7 μmol/g) with those for Ag/Al_2O_3 (I and II) (Fig. 3b). Therefore, this abundant O_2 desorption in O_2-TPD as well as an intense H_2 consumption in TPR occurring over Ag/Al_2O_3 (III) was related to the depletion of lattice oxygen during the phase transformation of amorphous hydroxy alumina to gamma type transition alumina. CO_2 desorption was attributed to carbonate species in Ag/Al_2O_3 (III) as evidenced by DRIFT (Fig. 2). In addition, metallic Ag appearing in Ag/Al_2O_3 (IV and V) was confirmed by UV–vis and TPR patterns (Figs. 1 and 4a). These data indicate that the structure and nature of the silver and amorphous support phases of Ag/Al_2O_3 (III) undergo drastic changes upon high-temperature calcination (≥800 °C).

In our previous NO + O_2-TPD study for perovskites, NO peaks related to nitrosyl and nitrate species with different thermal stabilities were observed [40]. α-O_2 was believed to oxidize adsorbed NO into NO_3^- species at anion vacancies of perovskites leading to a high-temperature NO desorption peak. These surface nitrates are regarded as important adspecies for SCR of NO in the presence of O_2 as documented in the literature [10,12]. A two-stage NO desorption from Ag/Al_2O_3 during NO + O_2-TPD was also reported by She and Flytzani-Stephanopoulos and attributed to the weakly chemisorbed NO (at $T < 300$ °C) and nitrate species (at 480 °C) [11]. Hence, the NO peaks at 179 and 354 °C from Ag/Al_2O_3 (I) after the adsorption of 3000 ppm NO and 1% O_2 were accordingly ascribed to the desorptions of nitrosyl and nitrate species, respectively. A high content of nitrate species (33–62 μmol/g) formed over $LaCo_{1-x}Cu_xO_3$ perovskites was found in our earlier NO + O_2-TPD investigation under the same TPD conditions [41]. Nevertheless, the nitrate species formed in the present study over Ag/Al_2O_3 (I) are in minor content (2.1 μmol/g). This result can be correlated to the lower oxidation ability of Ag/Al_2O_3 (I) compared to perovskites. Fortunately, the density of nitrate species formed over this Ag/Al_2O_3 (I) was significantly increased (42.3 μmol/g) by means of more gaseous oxygen introduction. This result allows to hope for a better performance in lean NO reduction.

4.2. Activity tests

4.2.1. Relationship between the nature and catalytic behavior of Ag catalysts derived from diverse alumina sources

Two maxima of 44% at 500 °C and 52% at 700 °C for N_2 yield obtained at 1% O_2 over Ag/Al_2O_3 (I) were found (Fig. 6). In the absence of silver and the presence of 1% O_2, the effectiveness of Al_2O_3 (I) for NO selective reduction into N_2 is low at $T < 600$ °C, nevertheless, N_2 yields at high-temperatures (>600 °C) achieved over Al_2O_3 (I) were close to those achieved over Ag/Al_2O_3 (I) in the same temperature range (not shown). A similar Ag effect on SCR performance of Al_2O_3 (I) was also observed in the presence of 10% oxygen (Fig. 5a). The low-temperature SCR of NO occurring over Al_2O_3 without the assistance of silver seems to be inhibited for some reason. It was found that the rates of NO_2 catalytic reduction by propene between Al_2O_3 and Ag/Al_2O_3 were similar, suggesting the promotion of SCR activity by Ag was realized by accelerating the NO oxidation to nitrate species (or NO_2) [12]. A bifunctional mechanism, in which Ag component forms NO_2 while Al_2O_3 reduces NO_2 to N_2, has been proposed [12]. According to our earlier studies [37,40], nitrate species formed over Cu containing perovskites were found to be highly reactive towards adsorbed C_3H_6 to form the organo-nitrogen intermediates which are important for N_2 production. In addition, Iglesias et al. suggested a new reaction pathway for propene activation by Ag which involved the generation of acrylate species as a partially oxidized active intermediate [32].

Attempts to correlate the catalytic performance of Ag-promoted alumina in NO-SCR reaction with the local structure of Ag cluster and alumina support have also been made by several authors [11,12,32]. Jen ascribed the larger $deNO_x$ activity for 2% Ag/Al_2O_3 to the support having a greater fraction of pore volumes in the range 25–100 Å or a narrower pore-size distribution [19]. It is known that the state of Ag is strongly depending on its loading [11,32]. Although all detected silver species are thought to be active in the SCR of NO_x, large silver oxide particles tend to give a lower SCR specific activity simultaneously with a higher oxidation of the hydrocarbon reductants [12,39].

The ratio of N_2 yield to C_3H_6 conversion ($Y(N_2)/X(C_3H_6)$) determined from data collected during the C_3H_6-SCR of NO as a function of temperature over the present alumina-based

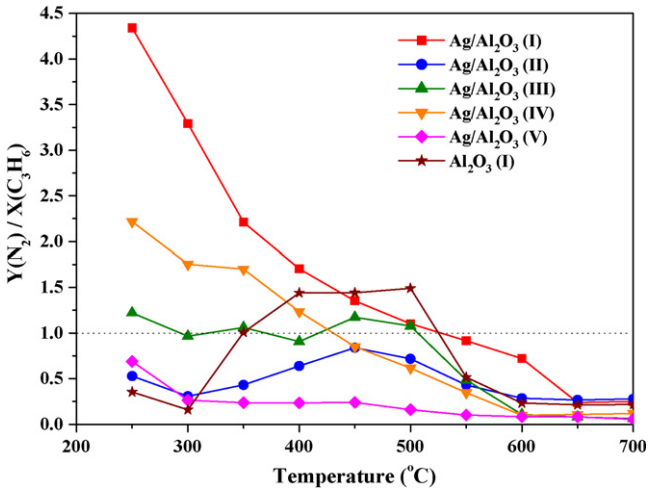

Fig. 9. Ratio of N_2 yield to C_3H_6 conversion in C_3H_6-SCR of NO over alumina-based samples. Conditions: GHSV = 30,000 h^{-1}, 1000 ppm NO, 3000 ppm C_3H_6, 10% O_2.

catalysts is shown in Fig. 9. This ratio decreases gradually due to a decline in N_2 yield together with an enhancement in C_3H_6 conversion at increasing temperature. In the low-temperature region of 300–500 °C Ag/Al_2O_3 (I and IV) showed a higher rate for NO selective reduction than propene oxidation giving $Y(N_2)/X(C_3H_6) > 1$, the opposite occurred for Ag/Al_2O_3 (II and V) showing $Y(N_2)/X(C_3H_6) < 1$ due to a largely nonselective combustion. The ionic Ag bound with the alumina forming an Ag–O–Al structure is believed to be vital for NO_x reduction since the SCR reaction rate is proportional to the number of Ag–O–Al sites [11]. The Ag–O–Al structures in alumina-supported Ag was found to be formed in a preparation by the sol–gel method [21] or upon dilute acid leaching to remove the larger Ag particles [11]. Both Ag/Al_2O_3 (I) and Ag/Al_2O_3 (IV) are prepared by an impregnation method but using Al sources containing –OH groups (such as AlOOH and $Al(OH)_3$), which also facilitates the formation of an Ag–O–Al local structure. Their good selectivity towards the formation of N_2 can thus correspond to the high density of Ag–O–Al species. On the contrary, the excellent oxidative abilities of Ag/Al_2O_3 (II) and Ag/Al_2O_3 (V) related to the formation of large Ag_mO ($m > 2$) crystallites are responsible for their high C_3H_6 conversion. The Ag–O–Al species are also believed to exist in Ag/Al_2O_3 (III) sample but they may be immersed in the alumina substrate thus not showing their SCR activities. The low surface area and amorphous structure of Ag/Al_2O_3 (III) limit its activity for both NO reduction and C_3H_6 oxidation resulting in a $Y(N_2)/X(C_3H_6)$ around 1. Thus, the Ag–O–Al local structure is crucial for SCR activity especially at low-temperature, while C_3H_6 conversion was essentially dependent on the oxidative properties of the prepared samples, which can be enhanced by loading more Ag or increasing the Ag particle size.

A γ-Al_2O_3 structure was obtained over Ag/Al_2O_3 (IV) after calcination at 800 °C of amorphous Ag/Al_2O_3 (III) leading to a clear enhancement in both N_2 yield and C_3H_6 conversion. This suggests that the high surface area γ-Al_2O_3 acting as a support is necessary for lean NO reduction. Ag/Al_2O_3 (V) was obtained by calcining Ag/Al_2O_3 (III) at 950 °C. It is surprising that the N_2 yield achieved over Ag/Al_2O_3 (V) was much lower while its C_3H_6 conversion was fully developed compared to Ag/Al_2O_3 (IV). This result may be explained by the formation of large-size Ag clusters during calcination at 950 °C as verified by UV–vis (Fig. 1) and H_2-TPR (Fig. 4a), yielding more readily reducible entities with a higher activity for nonselective propene oxidation.

The redox properties of Al_2O_3-based catalysts derived from various Al sources were investigated by O_2-TPD (Fig. 3a and b) and H_2-TPR (Fig. 4a and b) in this study showing an approximate oxidation capacity of Ag/Al_2O_3 (II and V) >Ag/Al_2O_3 (IV) >Ag/Al_2O_3 (I) > Ag/Al_2O_3 (III) or Al_2O_3 (I). The trend of C_3H_6 conversion (Fig. 5e), Ag/Al_2O_3 (II and V) >Ag/Al_2O_3 (IV and I) >Ag/Al_2O_3 (III) or Al_2O_3 (I), was similar to the order of oxidation capacity. CO was detected as a by-product in the effluents of NO reduction tests conducted on Ag/Al_2O_3 (I), Ag/Al_2O_3 (III) and Al_2O_3 (I) because of the relatively poor oxidation abilities of these catalytic materials leading to a partial oxidation of C_3H_6 (Fig. 5f). The percentage of CO in the exit stream therefore characterizes roughly the oxidation activity of silver catalysts. Based on our earlier investigations, carbon monoxide has a higher reactivity towards NO reduction than propene [40,42,43]. The ease of CO formation is thus likely a clue indicating a good performance for NO reduction. The low CO yields (<2%) of Ag/Al_2O_3 (II, IV and V) are related to their strong oxidative properties. The moderate CO formation over Ag/Al_2O_3 (I) was associated with its gentle oxidation capacity. Over the less oxidative Ag/Al_2O_3 (III) and Al_2O_3 (I) the CO product is obviously found at high-temperature.

According to the SCR mechanism previously proposed, ONCs are intermediates generated from the nitrate species and adsorbed propene [40]. The ease of ONCs formation is thus beneficial to N_2 production. The higher ONCs yields at low-temperature (<500 °C) for Ag/Al_2O_3 (I) and Ag/Al_2O_3 (IV) as observed in Fig. 5b are related with their high density of Ag–O–Al species associated with a better SCR activity. A decline in ONCs yield at >500 °C was ascribed to the further transformation of these compounds to N_2. The production of ONCs over Al_2O_3 (I) and Ag/Al_2O_3 (III) at low-temperature is difficult. A high thermal energy is thought to be necessary in the absence of Ag promoter or γ-phase structure. The intense ONCs yield of Al_2O_3 (I) and Ag/Al_2O_3 (III) occurring at >600 °C was attributed not only to the formation of these compounds at high-temperature but also to the poor ability to further transform those ONCs due to the low oxidation abilities of these catalysts. NO_2 yield was again consistent with the catalysts oxidative properties.

4.2.2. *Effect of oxygen and Ag loading on catalytic behaviors*

Compared to the corresponding values obtained in the presence of 10% O_2 (Fig. 5a–f), both N_2 yield and C_3H_6 conversion over Ag/Al_2O_3 (I) were noticeably lower (especially at low-temperatures) as the feed contained only 1% O_2 (Fig. 6). The ONCs and CO yields at 1% O_2 were shifted to high-temperature compared to those achieved at 10% O_2. The

formation of nitrate species was reported as an important step for SCR reaction [10]. The high reactivity of nitrate species towards propene was established by previous TPSR of NO + O_2 in C_3H_6/He tests conducted over a series of perovskites [40]. According to the present NO + O_2-TPD results, merely minor nitrate species (2.1 μmol/g) was formed over Ag/Al_2O_3 (I) during the coadsorption of 3000 ppm NO and 1% O_2. However, the increase of oxygen content in gas phase up to 10% led to a significant enhancement in the density of nitrate species formed over the same catalyst (42.3 μmol/g). The poor performance under 1% O_2 was thus ascribed to the scarcity of nitrate species leading to the difficulty of ONCs formation.

A further investigation of the effect of O_2 on catalytic activity at 500 °C over Ag/Al_2O_3 (I) under an atmosphere of 1000 ppm NO, 3000 ppm C_3H_6, and 0–10% O_2 is depicted in Fig. 7. This figure shows that O_2 acted as a promoter for Ag/Al_2O_3 (I) to improve both N_2 yield and C_3H_6 conversion under the tested O_2 concentration range (0–10%). A high concentration O_2 was indeed found to inhibit NO reduction by C_3H_6 over highly oxidized lanthanum cobaltites leading to the consumption of reductant via nonselective combustion [41]. This is therefore a real asset for silver catalysts. Over Ag/Al_2O_3 (I) along with the rapid increase in N_2 yield in the O_2 range of 0–4%, a significant ONCs formation was observed with a maximum at 2% O_2 and a decline at higher oxygen partial pressures (Fig. 7). This suggests that a little amount of oxygen is sufficient to facilitate the ONCs formation and more oxygen addition would accelerate the further ONCs conversion to N_2. Taking into account the low oxidative properties of Ag/Al_2O_3 (I), the promotion by oxygen of the catalytic performance was ascribed to the acceleration of ONCs formation via facilitating the NO_3^- generation and C_3H_6 transformation in agreement with previous reports [12,32].

It is known that the impregnation of alumina supports with a silver salt solution leads to a wide distribution of silver species depending on loading and kind of alumina used [44]. Based on Al_2O_3 (I) support, a series of catalysts with Ag loading of 0–6 wt% was prepared. Their activities were thereafter evaluated under the conditions of 1000 ppm NO, 3000 ppm C_3H_6, 10% O_2 and 450 °C as illustrated in Fig. 8. This results demonstrate the promoting effect of silver at intermediate loadings (2–3 wt%) on the SCR reaction, likely corresponding to highly dispersed Ag^+ cations (or fine Ag_2O nanoparticles) over alumina [20]. High Ag content in alumina likely led to the formation of Ag crystallites, which accelerates an unfavorable combustion of the reducing agent competing with the SCR of NO reaction. In the work of Meunier et al. the best deNO_x performance was achieved as 1 wt% silver was impregnated over a 115 m^2/g alumina [17]. The higher optimal Ag loading (2–3 wt%) in this study is likely assigned to the higher surface area of the alumina substrate (143 m^2/g) and preparation involving AlOOH, which results in a better dispersion of the silver component.

5. Conclusion

A series of alumina-supported Ag catalysts was prepared by impregnation starting with different Al sources such as AlOOH, Al_2O_3 and $Al(OH)_3$. The Ag/Al_2O_3 (I and II) catalysts, respectively, derived from AlOOH and Al_2O_3 exhibit a γ-phase structure and high surface areas ∼140 m^2/g, while Ag/Al_2O_3 (III) prepared from $Al(OH)_3$ after calcination at 500 °C shows an amorphous structure along with a low surface area of 35 m^2/g. The γ-Al_2O_3 phase can be obtained, simultaneously with an enhancement of surface area with values of 79 m^2/g for Ag/Al_2O_3 (IV) and 61 m^2/g for Ag/Al_2O_3 (V), by heating at a temperature higher than 800 °C. Because Ag/Al_2O_3 (V) underwent a calcination at extraordinarily high-temperature (950 °C), the sintering of Ag clusters over this catalyst became heavy together with the formation of silver aluminate.

Diverse Ag species were found over the prepared catalysts as evidenced by UV–vis, O_2-TPD and H_2-TPR. The hydroxyl groups of AlOOH and $Al(OH)_3$ precursors can facilitate the anchoring of Ag^+ ions on the alumina support through an exchange process in a colloid solution, finally, achieving a Ag–O–Al local structure. Those Ag–O–Al species are deemed as active sites for SCR of NO. A satisfying N_2 yield was thus obtained over Ag/Al_2O_3 (I and IV) associated with a strong interaction between Ag^+ ions and the alumina matrix. Big-size Ag_mO ($m > 2$) particles were formed over Ag/Al_2O_3 (II) via an impregnation method using γ-Al_2O_3 powder as support precursor. Owing to a lack of stabilization from the support, the silver oxide clusters were readily decomposed into Ag metal especially at high-temperature or large size. Those newly generated Ag atoms are believed to weaken the Ag–O bond yielding highly movable oxygens, which are essentially active for hydrocarbon oxidation.

The redox properties were determined by O_2-TPD and H_2-TPR showing an order for oxidation capacity of Ag/Al_2O_3 (II and V) > Ag/Al_2O_3 (V) > Ag/Al_2O_3 (I) > Ag/Al_2O_3 (III) and Al_2O_3 (I). The C_3H_6 conversions and NO_2 yields obtained over those materials are found to be strongly dependent on their oxidative properties.

The role of Ag is to improve the SCR performance mainly at low-temperature, possibly through promoting a NO oxidation to NO_2 (or nitrate species) as well as C_3H_6 activation, whereas this promoting effect is less significant at high-temperature (>600 °C). The poor activity of Ag/Al_2O_3 (III) for C_3H_6-SCR of NO at 10% O_2 was ascribed to the absence of γ-Al_2O_3 phase and low surface area (35 m^2/g). The catalytic performance for NO-SCR reaction can be enhanced to some extent by calcining at 800 °C to obtain Ag/Al_2O_3 (IV) samples with γ-Al_2O_3 structure and a surface area of 79 m^2/g.

As for Ag/Al_2O_3 (I) catalyst, O_2 always serves as a promoter to accelerate the rates for both NO reduction and C_3H_6 oxidation. SCR activity for alumina-based catalysts with various Ag contents was promoted by an optimal loading of 2–3 wt% silver, whereas the C_3H_6 conversion over those samples is favored at higher Ag loading.

Acknowledgment

Financial support of NSERC through its industrial chair program is gratefully acknowledged.

References

[1] S. Pischinger, Top. Catal. 30/31 (2004) 5.
[2] M. Iwamoto, S. Yokoo, K. Saaki, S. Kagawa, J. Chem. Soc., Faraday Trans. I 77 (1981) 1629.
[3] V.I. Parvulescu, P. Grange, B. Delmon, Catal. Today 46 (1998) 233.
[4] A. Shichi, A. Satsuma, T. Hattori, Chem. Lett. 30 (2001) 44.
[5] R. Burch, P.J. Millington, A.P. Walker, Appl. Catal. B: Environ. 4 (1994) 65.
[6] A. Satsuma, K. Shimizu, Prog. Energ. Combust. 29 (2003) 71.
[7] R. Burch, T.C. Watling, Appl. Catal. B: Environ. 11 (1997) 207.
[8] R. Burch, P.J. Millington, Catal. Today 26 (1995) 185.
[9] T. Miyadera, K. Yoshida, Chem. Lett. (1993) 1483.
[10] F.C. Meunier, V. Zuzaniuk, J.P. Breen, M. Olsson, J.R.H. Ross, Catal. Today 59 (2000) 287.
[11] X. She, M. Flytzani-Stephanopoulos, J. Catal. 237 (2006) 79.
[12] K.A. Bethke, H.H. Kung, J. Catal. 172 (1997) 93.
[13] H. He, R.D. Zhang, Y.B. Yu, J.F. Liu, Chin. J. Catal. 24 (2003) 788.
[14] G. Delahay, B. Coq, E. Ensuque, F. Figueras, Catal. Lett. 39 (1996) 105.
[15] M. Haneda, Y. Kintaichi, M. Inaba, H. Hamada, Catal. Today 42 (1998) 127.
[16] S. Satokawa, J. Shibata, K. Shimizu, A. Satsuma, T. Hattori, Appl. Catal. B: Environ. 42 (2003) 179.
[17] F.C. Meunier, R. Ukropec, C. Stapleton, J.R.H. Ross, Appl. Catal. B: Environ. 30 (2001) 163.
[18] L. Kundakovic, M. Flytzani-Stephanopoulos, Appl. Catal. A: Gen. 183 (1999) 35.
[19] H.-W. Jen, Catal. Today 42 (1998) 37.
[20] A. Martinez-Arias, M. Fernandez-Garcia, A. Iglesias-Juez, J.A. Anderson, J.C. Conesa, J. Soria, Appl. Catal. B: Environ. 28 (2000) 29.
[21] E. Seker, J. Cavataio, E. Guari, P. Lorpongpaiboon, S. Osuwan, Appl. Catal. A: Gen. 183 (1999) 121.
[22] K. Otsuka, R. Takahashi, I. Yamanaka, J. Catal. 185 (1) (1999) 182.
[23] A.D. Cowan, N.W. Cant, B.S. Haynes, P.F. Nelson, J. Catal. 176 (2) (1998) 329.
[24] T. Tanaka, T. Okuhara, M. Misono, Appl. Catal. B: Environ. 4 (1994) L1.
[25] T. Nakatsuji, R. Yasukawa, K. Tabata, K. Ueda, M. Niwa, Appl. Catal. B: Environ. 17 (1998) 333.
[26] N. Bogdanchikova, F.C. Meunier, M. Avalos-Borja, J.P. Breen, A. Pestrgakov, Appl. Catal. B: Environ. 36 (2002) 287.
[27] Z. Li, M. Flytzani-Stephanopoulos, J. Catal. 182 (1999) 313.
[28] A. Keshavaraja, X. She, M. Flytzani-Stephanopoulos, Appl. Catal. B: Environ. 27 (2000) L1.
[29] K. Shimizu, J. Shibata, H. Yoshida, A. Satsuma, T. Hattori, Appl. Catal. B: Environ. 30 (2001) 151.
[30] K. Arve, L. Čapek, F. Klingstedt, K. Eränen, L.-E. Lindfors, D.Y. Murzin, J. Dědeček, Z. Sobalik, B. Wichterlová, Top. Catal. 30/31 (2004) 91.
[31] B.A.A. Silberova, G. Mul, M. Makkee, J.A. Moulijn, J. Catal. 243 (2006) 171.
[32] A. Iglesias-Juez, A.B. Hungría, A. Martínez-Arias, A. Fuerte, M. Fernández-García, J.A. Anderson, J.C. Conesa, J. Soria, J. Catal. 217 (2003) 310.
[33] J.C. Bailar, H.J. Emeléus, S.R. Nyholm, A.F. Trotman-Dickenson, Comprehensive Inorganic Chemistry, Pergamon Press, Oxford, 1973, p. 97.
[34] M. Richter, U. Bentrup, R. Eckelt, M. Schneider, M.-M. Pohl, R. Fricke, Appl. Catal. B: Environ. 51 (2004) 261.
[35] L.P. Ren, W.L. Dai, X.L. Yang, Y. Gao, Z.K. Xie, K.N. Fan, Chin. J. Catal. 27 (2006) 115.
[36] S. Kaliaguine, A. van Neste, V. Szabo, J.E. Gallot, M. Bassir, R. Muzychuk, Appl. Catal. A: Gen. 209 (2001) 345.
[37] R.D. Zhang, A. Villanueva, H. Alamdari, S. Kaliaguine, Appl. Catal. A: Gen. 307 (2006) 85.
[38] T. Seiyama, Catal. Rev. Sci. Eng. 34 (1992) 281.
[39] T. Furusawa, K. Seshan, J.A. Lercher, L. Lefferts, K. Aika, Appl. Catal. B: Environ. 37 (2002) 205.
[40] R.D. Zhang, A. Villanueva, H. Alamdari, S. Kaliaguine, J. Catal. 237 (2006) 368.
[41] R.D. Zhang, A. Villanueva, H. Alamdari, S. Kaliaguine, Appl. Catal. B: Environ. 64 (2006) 220.
[42] R.D. Zhang, H. Alamdari, S. Kaliaguine, J. Catal. 242 (2006) 241.
[43] R.D. Zhang, A. Villanueva, H. Alamdari, S. Kaliaguine, J. Mol. Catal. A: Chem. 258 (2006) 22.
[44] T. Miyadera, Appl. Catal. B: Environ. 2 (1993) 199.